Journal of Materials Chemistry A

Accepted Manuscript

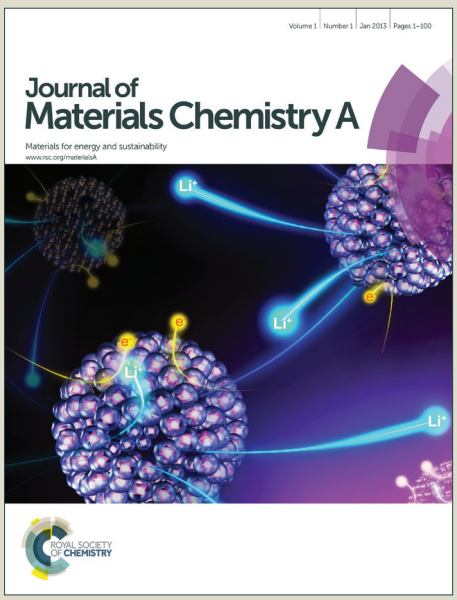

ROYAL SOCIETY OF CHEMISTRY

www.rsc.org/materialsA

Cite this: DOI: 10.1039/c0xx00000x

www.rsc.org/xxxxxx

ARTICLE TYPE

Enhanced HCHO gas sensing properties by Ag-loaded sunflower-like In_2O_3 hierarchical nanostructures

Shuangming Wang, Bingxin Xiao, Tianye Yang, Pan Wang, Chuanhai Xiao, Zhifang Li, Rui Zhao, and Mingzhe Zhang*

Received (in XXX, XXX) Xth XXXXXXXXX 20XX, Accepted Xth XXXXXXXXX 20XX

DOI: 10.1039/b000000x

Nanoscale Ag-loaded sunflower-like In_2O_3 hierarchical nanostructures are developed for HCHO detection. Such unique architectures are synthesized by an ambient temperature and pressure hydrolysis reaction combined with subsequent chemical reduction process. Morphology characterizations confirm that homodisperse nanochains assembled by nanoparticles along same direction are radially linked to a center to construct sunflower-like hierarchical nanostructures. Novel highly porous and branched structure of the 3D hierarchical architectures and the chemical and electronic sensitization effect of Ag nanoparticles endow Ag-loaded In_2O_3 nanostructures-based sensors with enhanced gas sensing performances in terms of fast response time (0.9 s), recovery time (14 s), high sensitivity and good sensing selectivity for 20 ppm HCHO. A multistage reaction formation mechanism of the sunflower-like hierarchical nanostructures, and the morphology-dependent sensing mechanism are proposed.

1. Introduction

Nanomaterials with tailored structure, size and morphology have been extensively studied as chemical sensor materials,[1,2] whose need has been heightened with increasing concerns of air pollution and noxious gas on human health and safety.[3] In particular, three dimensional (3D) hierarchical complex nanostructures assembled with nanoparticles, nanopetals, nanowires, nanorods, and so forth, are promising candidates for gas sensors.[4-7] To find and investigate the novel hierarchical nanostructures is still an interesting task not only in answering basic research questions but also in technological application.[8] Until now, many efforts have been devoted to the fabrication of the hierarchical nanostructures from nanoscale building blocks.[9,10] However, it is worth noting that simple and facile fabrication of functional hierarchical nanostructures without stern experiment conditions or the emission of noxious gas still remains a challenge.

In_2O_3, as an important n-type semiconductor with a wide band gap of about 3.6 eV, has been used in various applications, such as gas sensors, solar cells, optoelectronic devices and catalysis.[11-14] To enhance the functional properties of In_2O_3 nanostructures, it is essential to control its size and morphology. Especially for application as gas sensors, high surface to volume ratios and nano-scale dimension are the key factors to determine the gas response.[15] Recently, In_2O_3 with high specific surface areas and hierarchical structures have been shown to be promising for sensing applications. Moreover, if noble metal nanoparticles can be integrated into the 3D hierarchical nanostructures, enhanced activity and sensitivity can be expected because they can improve the adsorption of gas molecules and accelerate the electron exchange between the sensors and the target gas.[16]

Herein, 3D sunflower-like In_2O_3 hierarchical nanostructures are successfully prepared by the calcination of $In(OH)_3$ precursors, which are synthesized through a simple hydrolysis reaction. The present method is facile, fast, economical and environmentally friendly. In particular, the greatest advantage of this method is ambient temperature and pressure. The as-prepared In_2O_3 hierarchical nanostructures present unique sunflower-like morphology with rough and porous surfaces and diameters of 520-580 nm, whose size and contour is rare for the reported hierarchical structures.[17,18] Furthermore, novel 3D Ag-loaded sunflower-like hierarchical nanostructures are designed for high sensitive gas sensors by combining the advantages of In_2O_3 hierarchical structures with a high surface area and the synergistic effect of Ag nanoparticles. The sensors based on Ag-loaded In_2O_3 hierarchical nanostructures show fast response time (0.9 s), recovery time (14 s), high sensitivity and good sensing selectivity for 20 ppm HCHO.

2. Experimental section

2.1 Fabrication of 3D sunflower-like $In(OH)_3$ and In_2O_3 hierarchical nanostructures

All the reagents (analytical-grade purity) were used as purchased without further purification. Deionized water was used in the experiments. In a typical synthesis for $In(OH)_3$, 43 mg $In(NO_3)_3 \cdot 4.5\ H_2O$ was dissolved in 30 ml deionized water with stirring for 30 min, then 80 mg cetyltrimethyl ammonium bromide (CTAB) was added into transparent solution. After further stirring for 1 h, the freshly prepared 25 ml 0.05 mol/L $NaBH_4$ aqueous solution was added dropwise to the aboved mixed solution. After being stirred for 2 h, the ivory-white precipitates $In(OH)_3$ were collected by centrifugation, washed several times with deionized water and absolute ethanol, respectively, and dried in air at 60 ^oC for 12 h. Finally, the yellowish sunflower-like In_2O_3 hierarchical nanostructures were obtained by calcining the ivory-white precipitates $In(OH)_3$ at 600 ^oC for 3 h in air. The heating rate was controlled at 1 $^oC\ min^{-1}$.

2.2 Synthesis of Ag-loaded sunflower-like In_2O_3 hierarchical structures

Ag nanoparticles were prepared by a chemical reduction method.[19] In a typical procedure, 3 ml 0.02 mol/L $NaBH_4$ aqueous solution (-2 ^oC) was added dropwise to an aqueous solution containing 1 ml 0.06 mol/L $C_6H_5Na_3O_7 \cdot 2H_2O$ and 100 ml 0.0005 mol/L $AgNO_3$ under vigorous stirring. After further stirring for 1 min, the solution was maintained to react for 1 h without stirring. The black precipitates were collected by centrifugation and washed with deionized water. Subsequently, the black precipitates were dispersed by 1 ml deionized water and then 80 mg In_2O_3 nanomaterials was added. The mixed solution was put in the ultrasonic device for 2 h and then dried at 60 ^oC to remove the solvent for further use.[20] The weight percentage of Ag in the composites is 6%.

2.3 Fabrication of gas sensors

The as-prepared pure In_2O_3 (0.08 g) and 6 wt% Ag-loaded In_2O_3 (0.08 g) nanomaterials were uniformly dispersed into distilled water (about 0.2 ml) to form a paste, respectively. Then the paste was painted on the surface of a ceramic tube (outer diameter = 1.35 mm, length = 4 mm) on which a pair of gold electrodes was previously printed. A Ni-Cr heating wire (diameter = 0.5 mm, resistance = 35 Ω) was inserted into the tube to heat the gas sensor directly. In order to improve their stability and repeatability, the gas sensors were sintered at 350 ^oC for 10 h in air. The sensor based on 6 wt% Ag-loaded In_2O_3 was named as the Ag-loaded In_2O_3 in the whole manuscript. To investigate the influence of Ag loading ratio for gas sensing response, two contrast gas sensors based on In_2O_3 with various contents of Ag (3 wt% and 9 wt%) were prepared and named as CS1 and CS2, respectively.

The sensor was welded on a socket and the electrical properties of the sensor were measured by a CGS-8 intelligent gas sensing analysis system. The sensor response was defined as $S = R_a/R_g$. Here, R_a and R_g were the resistances of the sensors in the air and target gas, respectively. The response and recovery time was defined as the time taken by the sensors to achieve 90% of the total resistance change in the case of adsorption and desorption, respectively.

2.4 Characterization

FESEM images were obtained using a JEOL JSM-6700F microscope. TEM, HRTEM, SAED and mapping images were obtained on a JEOL JEM-2200FS microscope. The crystal phases of the synthesized samples were characterized by X-ray powder diffraction (XRD, Rigaku D/max-Ra). Room temperature UV–vis spectra were recorded on UV-3150 spectrophotometer.

3. Results and discussion

3.1 Morphology and composition analysis

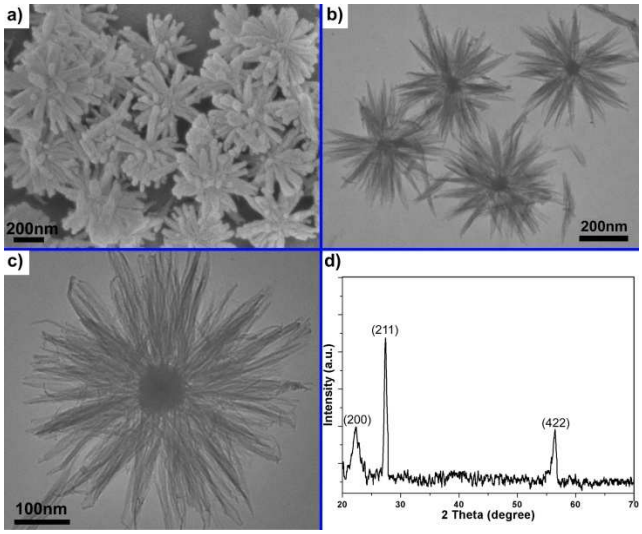

Fig. 1 (a) A low-magnification SEM image, (b) enlarged TEM image, (c) high-magnification TEM image and (d) XRD pattern of the as-prepared sunflower-like $In(OH)_3$ hierarchical nanostructures.

Fig. 1a shows a panoramic FESEM image of the sunflower-like $In(OH)_3$ hierarchical nanostructures. It can be clearly seen that numerous rod-shaped branches are connected into one center

point and are radially arranged to form a flower-like shape, which is named as the sunflower-like hierarchical nanostructures. The concept of the sunflower-like nanostructures can be clearly understood by TEM images in Fig. 1b and 1c. As shown in the TEM images, the center point (about 90 nm in diameter) and surrounding homodisperse nanobranches can be clearly observed. The XRD analysis is performed to investigate the crystal phase of as-prepared ivory-white precipitates. All diffraction peaks can be well assigned to those of $In(OH)_3$ (JCPDS No.76-1463). No diffraction peaks from any other impurities are detected.

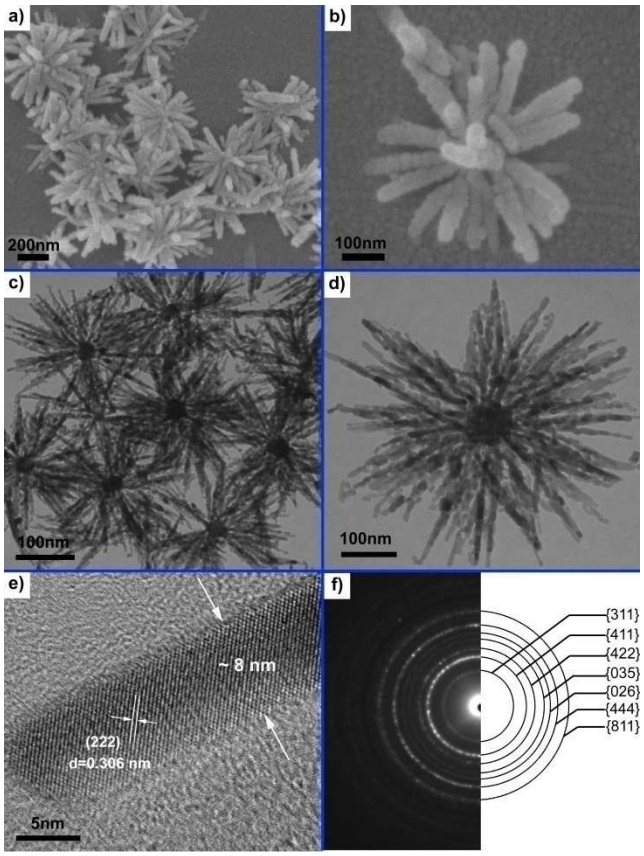

Fig. 2 (a-b) A low-magnification and enlarged FESEM image, (c-d) low-magnification and enlarged TEM image, (e) HRTEM image and (f) SAED pattern of the as-synthesized sunflower-like In_2O_3 hierarchical nanostructures.

After annealing the as-prepared $In(OH)_3$ precursors at 600 ^oC for 3 h under ambient pressure, the sunflower-like In_2O_3 hierarchical nanostructures are obtained, as shown in Fig. 2a and 2c. It can be found that the dehydration of the $In(OH)_3$ precursors does not alter flower-like shape with the diameters ranging from 520 nm to 580 nm, but results in structure conversion of nanobranches from nanorods to nanochains. As expected, the central portion of the hierarchical nanostructures is darker than that of the edge, further confirming the sunflower-like interior of the unique self-wrapped chain-like array, which has been demonstrated for the first time. Furthermore, Fig. 2b and 2d reveal the details of such hierarchical nanostructures. Each nanochain presents a porous surface, shows similar widths (~ 8 nm) and lengths (~ 220 nm), and consists of numerous nanoparticles that are regularly assembled along the same direction. A typical HRTEM image (Fig. 2e) of a single fine nanochain clearly shows the lattice fringes of In_2O_3. Lattice fringes spaced by 0.306 nm correspond to In_2O_3 (222) lattice planes. The selected-area electron diffraction (SAED) image shown in Fig. 2f, confirms the In_2O_3 hierarchical structure is of polycrystalline structure. It is noteworthy that the visual difference between the SEM and TEM images should originate from a higher resolution of transmission electron microscope than that of scanning electron microscope.

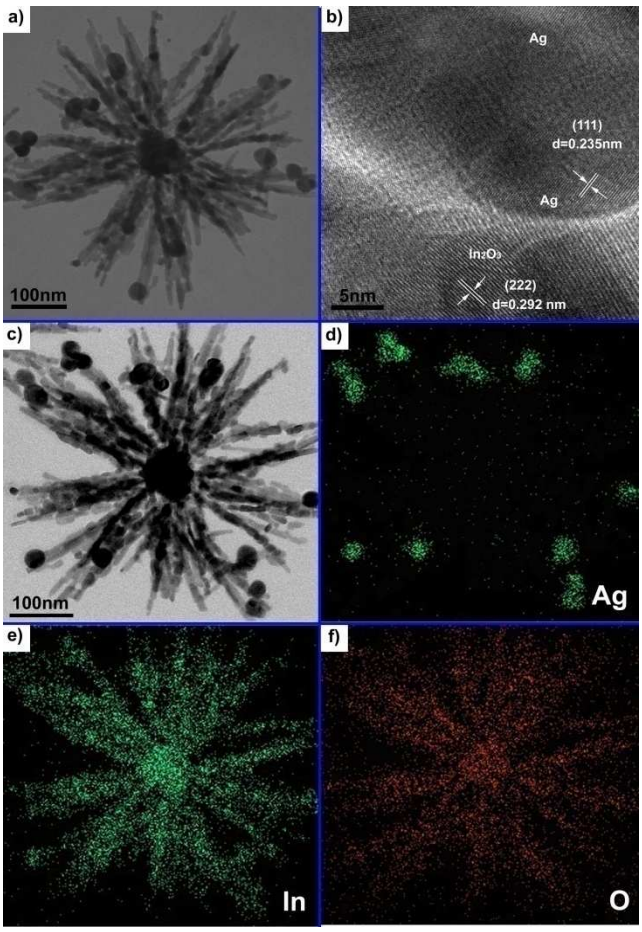

Fig. 3 (a) A typical TEM image, (b) HRTEM image, (c) bright field image (from STEM pattern) and (d-f) elemental mapping images of Ag, In and O, respectively of the Ag-loaded sunflower-like In_2O_3 hierarchical nanostructures.

After Ag nanoparticles are decorated onto the In_2O_3 hierarchical nanostructures, the morphology of the product is

characterized by a TEM image, as shown in Fig. 3a. It can be obviously seen that Ag nanoparticles with a diameter of 20-45 nm are well pinned on the surfaces of the In_2O_3 hierarchical nanostructures, which will be helpful for the enhancement of gas-sensing properties. HRTEM image from Fig. 3b reveals the interplanar spacing of about 0.292 nm, corresponding to the (222) plane of In_2O_3, while the interplanar spacing of 0.235 nm can be assigned to the (111) plane of Ag. Furthermore, the sharp interface indicates the existence of strong electronic interaction between Ag nanoparticles and In_2O_3 nanostructures.[21] The locations of Ag nanoparticles can be more clearly observed by the bright field image of STEM pattern (Fig. 3c). Moreover, the spatial distribution of different compositional elements of the Ag-loaded In_2O_3 sample are clarified by the elemental mapping of Ag, In, O, respectively, as shown in Fig. 3d-f. As expected, the distribution of In and O elements is homogeneous and exhibits a sunflower-like structure. In Fig. 3d, Ag element is mainly dispersed on the upper part of the hierarchical structure. These results demonstrate that Ag nanoparticles are successfully loaded onto the surface of sunflower-like In_2O_3 hierarchical nanostructures and the unique sunflower-like shape does not change with the decoration of Ag.

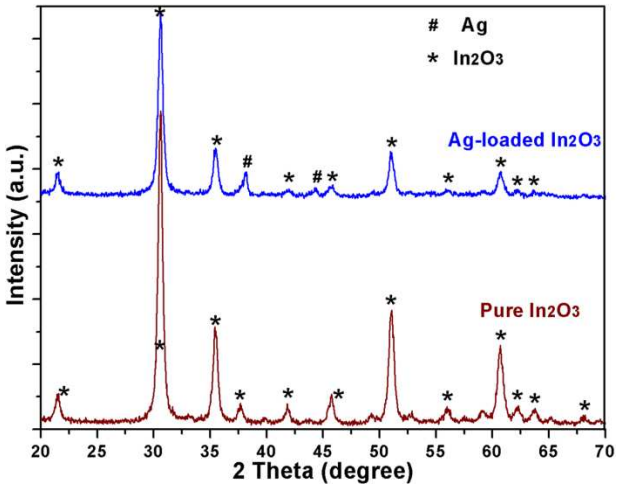

Fig. 4 XRD patterns of the pure and Ag-loaded sunflower-like In_2O_3 hierarchical nanostructures.

The crystal phase of the pure and Ag-loaded sunflower-like In_2O_3 hierarchical nanostructures is characterized by XRD. Fig. 4 shows the XRD patterns of the pure and Ag-loaded sunflower-like In_2O_3 hierarchical nanostructures. The peaks of the In_2O_3 (JCPDS No. 76-0152) can be observed from both samples. For Ag-loaded In_2O_3 samples, two additional peaks (marked with #) can be assigned to Ag peaks (JCPDS No.87-0597). No impurity phases are observed from the XRD patterns, which further confirm the excellent purity of both products.

3.2 Formation mechanism

FESEM and TEM images have demonstrated that the sunflower-like hierarchical nanostructures remain during the phase transformation from $In(OH)_3$ to In_2O_3. Thus, the formation process of $In(OH)_3$ hierarchical nanostructures is studied to understand In_2O_3 fabrication mechanism.

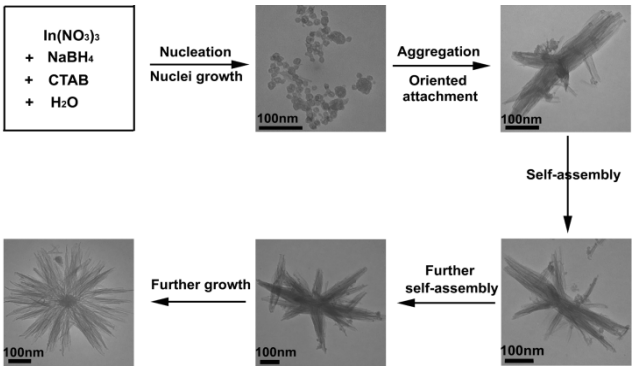

Fig. 5 Schematic illustrations of the growth process of the sunflower-like $In(OH)_3$ hierarchical nanostructures.

In the present aqueous system, each ingredient is essential and indispensable to the final formation of the sunflower-like $In(OH)_3$ hierarchical nanostructures. On the one hand, the deionized water reacts with $NaBH_4$ to produce OH^-.[22] Moreover, nitrate ions (NO_3^-) from $In(NO_3)_3$ also can react with the deionized water to generate OH^-.[23] Thus, with the addition of $NaBH_4$ aqueous solution, In^{3+} ions will combine OH^- to form $In(OH)_3$. Because of the existence of OH^- groups, the electrostatic and hydrogen bonds may be the main driving forces for the self-assembly process.[24,25] On the other hand, after $In(OH)_3$ nanocrystals are obtained, CTAB may act as "soft" template and selectively adsorb on the circumference of $In(OH)_3$.[26,27]

On the basis of the information gathered from the above results and analysis, a multistage growth mechanism of the sunflower-like $In(OH)_3$ hierarchical nanostructures can be proposed and is schematically illustrated in Fig. 5. At the early stage of the reaction, the primary $In(OH)_3$ nanocrystals are formed by the conventional nucleation and a subsequent crystal growth process, relating to both the anisotropic $In(OH)_3$ crystal structure and the complex solution conditions. From a thermodynamics perspective, the primary nanocrystals formed through hydrolysis are unstable. Then, many neighboring primary $In(OH)_3$ nanoparticles further grow into dendritic nanocrystals by oriented aggregation to greatly reduce the interfacial energy.[28] Subsequently, as the

synthesis reaction goes on, the star-like nanostructures are gradually taken shape through further the oriented attachment and self-assembly.[29,30] Finally, the star-like nanostructures continue to grow by combining with the remaining $In(OH)_3$ nanocrystals to form 3D sunflower-like hierarchical nanostructures.

3.3 Optical properties

The UV-vis absorption spectra of the pure and Ag-loaded sunflower-like In_2O_3 hierarchical nanostructures are further clarified and shown in Fig. 6. The UV absorption around 270 nm of the pure In_2O_3 hierarchical nanostructures exhibits a distinct blue shift compared with the absorption around 330 nm of the bulk In_2O_3, which is probably attributable to the weak quantum confinement effect.[31-33] Furthermore, the absorption study obviously reveals that the as-prepared In_2O_3 hierarchical nanostructures are transparent in the visible region. However, compared with pure sunflower-like In_2O_3 hierarchical nanostructures, the absorbance peak edges of the Ag-loaded In_2O_3 nanomaterials have an evident red-shift by coupling Ag nanoparticles on the surface of In_2O_3 hierarchical nanostructures. The absorption edge is greatly extended to the visible light region due to the surface plasmon response absorption of Ag nanoparticles.[34, 35]

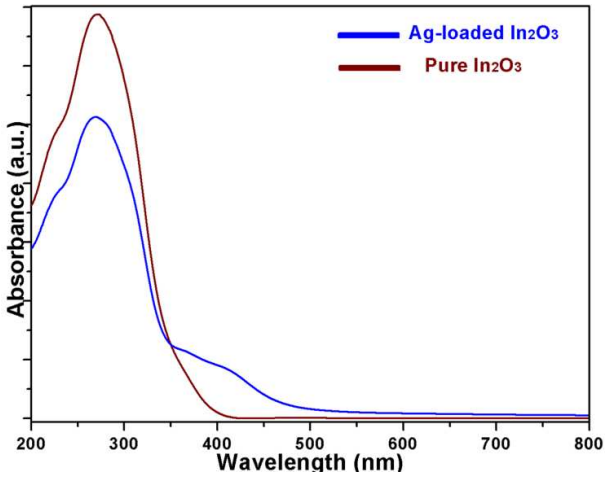

Fig. 6 UV-vis absorption spectra of the pure and Ag-loaded sunflower-like In_2O_3 hierarchical nanostructures.

3.4 Gas sensing properties

In_2O_3 has been proved to be a good sensing material for harmful and toxic gases due to its excellent semiconducting and mature fabrication technology. In the gas sensing study, the operating temperature is important for the investigation on gas sensing properties due to its great influence on the surface state of sensing materials, as well as the contact reactions during the gas sensing process. Fig. 7a shows the responses of two sensors based on pure and Ag-loaded In_2O_3 to 20 ppm HCHO at different operating temperatures. Obviously, the response of each sensor is strongly dependent on the operating temperature. Each sensor has an optimal operating temperature, at which the sensor exhibit the highest response to HCHO gas. At various temperatures, the sensors based on Ag-loaded In_2O_3 present higher response to HCHO compared with that of sensors using pure In_2O_3. It can be found that pure In_2O_3-based sensors show the maximum response of 4.2 at 240 ^oC while Ag-loaded In_2O_3-based sensors show a maximum response of 12.3 at 200 ^oC. Although Ag-loaded In_2O_3-based sensors present slightly high response at 220 ^oC (11.8) and 200 ^oC (12.3) than that at 240 ^oC (11.3), the sensors exhibit longer recovery time at 220 and 200 ^oC. Thus, 240 ^oC is chosen as the optimal operating temperature, at which Ag-loaded In_2O_3-based sensors exhibit fast response (0.9 s), recovery time (14 s) and high response (11.3) for 20 ppm HCHO.

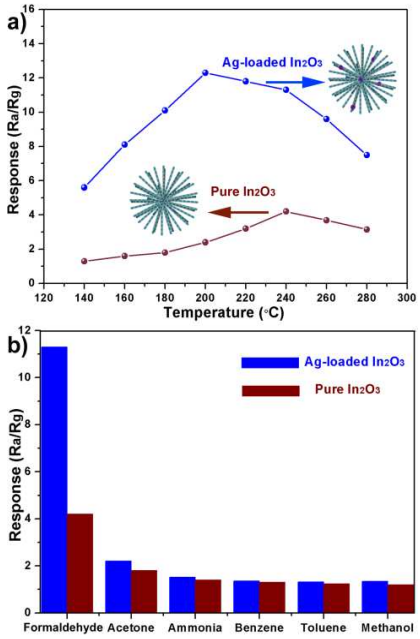

Fig. 7 (a) Responses of the pure and Ag-loaded sunflower-like In_2O_3 hierarchical nanostructures to 20 ppm HCHO at different operating temperatures, (b) responses of the pure and Ag-loaded sunflower-like In_2O_3 hierarchical nanostructures to 20 ppm various testing gases.

Gas sensors for practical applications are required not only to have high sensor response, but also very good selectivity to the targeted gases. Therefore, the responses of the sensors based on the pure and Ag-loaded In_2O_3 to 20 ppm formaldehyde (HCHO), acetone (C_3H_6O), ammonia (NH_3), benzene (C_6H_6), toluene

(C_7H_8) and methanol (CH_3OH) are also measured at 240 °C. The responses of the Ag-loaded nanostructures sensor to six gases are all improved compared with the pure In_2O_3 nanostructures, and the largest increase is observed for HCHO, as shown in Fig. 7b. Such a significant improvement of the sensing performance of the Ag-loaded In_2O_3 hierarchical nanostructures can be attributed to the modification of Ag nanoparticles. Moreover, the response values are all less than 2 for other gases, indicating that both sensors have very good selectivity for HCHO vapor, which is mainly attributed to the enhanced reaction between the absorbed oxygen and the HCHO at the optimum operating temperature.[36] The possible reaction of HCHO with the adsorbed oxygen can be explained as follows: $HCHO + 2O^-(ad) \rightarrow CO_2 + H_2O + 2e^-$.[37]

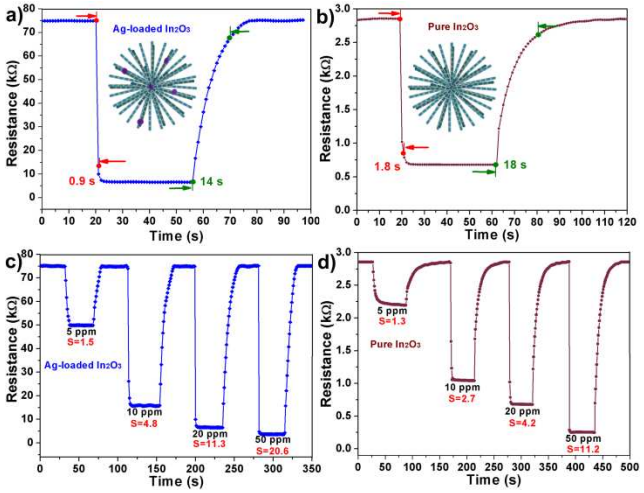

Fig. 8 (a-b) Response transients of Ag-loaded and pure In_2O_3 sensors to 20 ppm HCHO at 240 °C, (c-d) the dynamic response of Ag-loaded and pure In_2O_3 sensors to different HCHO concentrations (5-50 ppm) at 240 °C.

Fig. 8a and 8b shows the response transients of Ag-loaded and pure In_2O_3 sensors exposed to 20 ppm HCHO at 240 °C, respectively. The response time and recovery time of Ag-loaded and pure In_2O_3-based sensors are calculated to be 0.9 s and 14 s, and 1.8 s and 18 s, respectively. It can be seen that the Ag-loaded In_2O_3-based sensors own faster response and recovery speeds, besides higher response value. Fig. 8c and 8d depicts the representative dynamic responses of Ag-loaded and pure In_2O_3-based sensors to different HCHO concentrations (5-50 ppm) at 240 °C, respectively. It is obviously found that the response value of the Ag-loaded In_2O_3 increases rapidly with the increase of HCHO concentration and it reaches 11.3 for 20 ppm HCHO, which is an almost threefold enhancement in sensitivity compared with that of the pure In_2O_3 nanostructures. Furthermore, for each concentration, Ag-loaded In_2O_3-based sensors exhibit higher sensitivity, faster response time and recovery time than that of pure In_2O_3. Furthermore, it has been reported that the loaded Ag ratio of the composites can influence gas sensing performances. Thus, for comparison, response transients of the CS1 and CS2 with different loading amounts of Ag (3 wt% and 9 wt%) to 20 ppm HCHO at 240 °C are tested (Fig. S1). By combining the results of Fig. 8, the typical Ag loading ratio-dependent sensing behavior is obviously observed. And the responses of pure In_2O_3, CS1 (3 wt%), Ag-loaded In_2O_3 (6 wt%) and CS2 (9 wt%) are 4.2, 5.5, 11.3 and 6.4, respectively. The 6 wt% Ag-loaded In_2O_3 sensor shows the largest response (11.3), in comparison with the pure In_2O_3, CS1 and CS2 sensor. Further increasing the Ag content (9 wt%), however, decreases the gas sensitivity. These results further indicate that the Ag decoration of nanomaterials is one of the most effective methods for improving the sensing performance and the as-prepared Ag-loaded In_2O_3 hierarchical nanostructures is a very promising candidates for fabricating high performance gas sensors to detect HCHO gas.

3.5 Gas sensing mechanism

In_2O_3, as an n-type metal oxide semiconductor, exhibits a resistance change through the thickness of the depletion layer that varies according to the mass of oxygen absorbed to the surface.[38] Fig. 9 presents the gas sensing mechanism schematic illustration of 3D sunflower-like Ag-loaded In_2O_3 hierarchical nanostructures. When the In_2O_3 is exposed to an air atmosphere, as shown in Fig. 9a, oxygen molecules can be adsorbed on the In_2O_3 surface and capture free electrons from the conduction band of In_2O_3 to form chemisorbed oxygen ions. As a result, the equilibration of the chemisorptions process leads to the generation of the depletion layers on the surface regions and eventually increases the In_2O_3 resistance. When the In_2O_3 is exposed to the HCHO gas, as depicted in Fig. 9b, these molecules can react with the oxygen ions and release the trapped electrons back to the conduction band, resulting in a decreased resistance of In_2O_3.

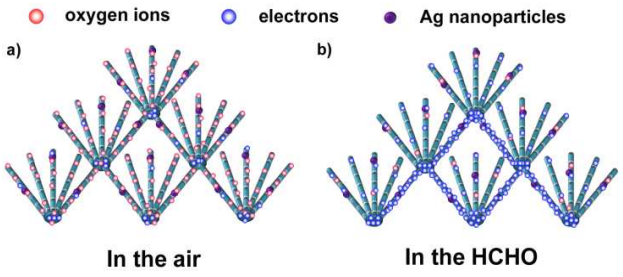

Fig. 9 Schematic illustration of the gas sensing mechanism of 3D sunflower-like Ag-loaded In_2O_3 hierarchical nanostructures.

Such an excellent response and recovery behavior is infrequent in the conventional In_2O_3 sensors. The enhanced gas sensing properties is likely due to the perfect sunflower-like hierarchical nanostructures and the catalytic effect of Ag additives. On one hand, the unique 3D sunflower-like hierarchical nanostructures own numerous radial nanobranches with rough surfaces, which provide highly exposed surfaces and more pathways for electron exchange during gas diffusion/molecule capture and surface reaction. Moreover, it has been reported that only the primary particles near the surface region of the materials contribute to the gas sensing reaction and the inner part remains inactive.[39, 40] Thus, the slender nanobranches ensure that whole hierarchical nanostructures can fully involve gas sensing. More importantly, the special sunflower-like nanostructures make the sensors construct a 3D "satellite signal receiver" networks for the different testing gases, which can translate the gas recognition into an electrical signal more easily and rapidly and then transport electrons effectively.

On the other hand, the appropriate loaded Ag plays chemical and electronic sensitization role in the gas sensing performances. The chemical sensitization promotes the gas response reaction by the dissociation of reducing gases (HCHO) via a spillover effect.[41] And the electronic sensitization greatly improves the direct electrons exchange between the In_2O_3 and the noble metal (Ag) additives.[42] However, the heavy Ag loading will cause electrons to conduct along the metallic Ag nanoparticles regardless of chemoresistive variation, deteriorating the gas response.[15]

4. Conclusions

In summary, novel Ag-loaded sunflower-like In_2O_3 hierarchical nanostructures are successfully synthesized by two-step simple and facile solution-based method. The as-prepared In_2O_3 samples consist of 3D sunflower-like In_2O_3 hierarchical nanostructures with porous surfaces and Ag nanoparticles. Numerous chain-shaped nanobranches are connected into one center disk and radially arranged to form a sunflower-like morphology. The Ag-loaded In_2O_3 hierarchical nanostructures sensors show fast response (0.9 s), recovery (14 s) and high response (11.3) towards 20 ppm HCHO. The excellent sensing performances are attributed to the particular flower-like morphology and the catalytic effect of Ag nanoparticles. The results evidently prove that the effective integration of noble metal nanoparticles with hierarchical semiconductor nanostructures will be helpful for the development of new sensing materials.

Acknowledgements

This work was funded by the National Science Foundation of China, Nos. 11174103 and 90923032, and Specialized Research Fund for the Doctoral Program of Higher Education of China, No. 20130061110012.

Notes and references

*State Key Laboratory of Superhard Materials, Jilin University, Changchun 130012, People's Republic of China. *Corresponding Author, E-mail address: zhangmz@jlu.edu.cn.*

1 Y.S. Li, J. Xu, J.F. Chao, D. Chen, S.X. Ouyang, J.H. Ye and G.Z. Shen, *J. Mater. Chem.*, 2011, **21**, 12852.

2 L.N. Han, D.J. Wang, J.B. Cui, L.P. Chen, T.F. Jiang and Y.H. Lin, *J. Mater. Chem.*, 2012, **22**, 12915.

3 S.L. Bai, K.W. Zhang, R.X. Luo, D.Q. Li, A.F. Chen and C. C. Liu, *J. Mater. Chem.*, 2012, **22**, 12643.

4 J.Y. Liu, T. Luo, F.L. Meng, K. Qian, Y.T. Wan and J.H. Lou, *J. Phys. Chem. C*, 2010, **114**, 4887.

5 D. Chen, J. Xu, Z. Xie and G.Z. Shen, *ACS Appl. Mater. Interfaces*, 2011, **3**, 2112.

6 Q. Wang, L.S. Zhang, J.F. Wu, W.D. Wang, W.G. Song and W. Wang, *J. Phys. Chem. C*, 2010, **114**, 22671.

7 Z.Y. He, Z.H. Chen, Y.G. Li, Q.H. Zhang and H.Z. Wang, *CrystEngComm*, 2011, **13**, 2557.

8 C.Q. Wang, D.R. Chen, X.L. Jiao and C.L. Chen, *J. Phys. Chem. C*, 2007, **111**, 13398.

9 G.X. Zhu, H. Xu, Y.Y. Xiao, Y.J. Liu, A.H. Yuan and X.P. Shen, *ACS Appl. Mater. Interfaces*, 2012, **4**, 744.

10 J. Xu, Y.S. Li, H.T. Huang, Y.G. Zhu, Z.R. Wang, Z. Xie, X.F. Wang, D. Chen and G.Z. Shen, *J. Mater. Chem.*, 2011, **21**, 19086.

11 X.M. Xu, P.L. Zhao, D.W. Wang, P. Sun, L. You, Y.F. Sun, X.S. Liang, F.M. Liu, H. Chen and G.Y. Lu, *Sens. Actuators, B*, 2013, **176**, 405.

12 R. Katoh, A. Furube, T. Yoshihara, K. Hara, G. Fujihashi, S. Takano,S. Murata, H. Arakawa and M. Tachiya, *J. Phys. Chem. B*, 2004, **108**, 4818.

13 S.Y. Han, G.S. Herman and C.H. Chang, *J. Am. Chem. Soc.*, 2011, **133**, 5166.

14 L.Y. Chen, Y. Liang and Z.D. Zhang, *Eur. J. Inorg.Chem.*, 2009, **2009**, 903.

15 L. Xu, R.Q. Xing, J. Song, W. Xu and H.W. Song, *J. Mater. Chem. C*, 2013, **1**, 2174.

16 Y. Wang, Y.M. Wang, J.L. Cao, F.H. Kong, H.J. Xia, J. Zhang, B.L. Zhu, S.R. Wang and S.H. Wu, *Sens. Actuators, B*, 2008, **131**, 183.

17 H. N. Hieu, N. M. Vuong, H. Jung, D.M. Jang, D. Kim, H. Kim, *J. Mater. Chem.*, 2012, **22**, 1127.

18 X.M. Xu, D.W. Wang, W.B. Wang, P. Sun, J. Ma, X. S. Liang, Y.F. Sun, Y.G. Ma and G.Y. Lu, *Sens. Actuators, B*, 2012, **171**, 1066.

19 K.H. Chen, Y.C. Pu, K.D. Chang, Y.F. Liang, C.M. Liu, J.W. Yeh, H.C. Shih and Y.J. Hsu, *J. Phys. Chem. C*, 2012, **116**, 19039.

20 P.B. Liu, Y. Huang and L. Wang, *Mater. Lett.*, 2013, **97**, 173.

21 Y.L. Yu, Y.Y. Zhao, H.Y. Sun and M. Ahmad, *Mater. Lett.*, 2013, **108**, 41.

22 H. Y. Lai and C.H. Chen, *J. Mater. Chem.*, 2012, **22**, 13204.

23 G.L. Cui, L. Gao, B.B. Yao, S.M. Wang, P.H. Zhang and M.Z. Zhang, *Electrochem. Commun.*, 2013, **30**, 42.

24 S.H. Ran, Y.G. Zhu, H.T. Huang, B. Liang, J. Xu, B. Liu, J. Zhang, Z. Xie, Z.R. Wang, J.H. Ye, D. Chen and G.Z. Shen, *CrystEngComm*, 2012, **14**, 3063.

25 L.P. Xu, Y.S. Ding, C.H. Chen, L.L. Zhao, C. Rimkus, R. Joesten and S.L. Suib, *Chem. Mater.*, 2008, **20**, 308.

26 J. Yang, C.K. Lin, Z.L. Wang and J. Lin, *Inorg. Chem.*, 2006, **45**, 8973.

27 M. Yang, H.P. You, Y.J. Huang, G. Jia, Y.H. Song, N. Guo, K. Liu, Y. H. Zheng and H.J. Zhang, *CrystEngComm*, 2010, **12**, 2865.

28 H.J. Song, X.H. Jia and X.Q. Zhang, *J. Mater. Chem.*, 2012, **22**, 22699.

29 H.F. Liang, B.B. Xu and Z.C. Wang, *Mater. Chem. Phys.*, 2013, **141**, 727.

30 H.Y. Lai, T.H. Chen and C.H. Chen, *CrystEngComm*, 2012, **14**, 5589.

31 Z. Guo, J.Y. Liu, Y. Jia, X. Chen, F.L. Meng, M.Q. Li and J.H. Liu, *Nanotechnology*, 2008, **19**, 345704.

32 C.L. Chen, D.R. Chen, X.L. Jiao and S.H. Chen, *J. Phys. Chem. C*, 2007, **111**, 18039.

33 S.J. Luo, D.N. Yang, J.L. Zhuang and K.M. Ng, *CrystEngComm*, 2013, **15**, 8065.

34 T. Wang, Z.B. Jiao, T. Chen, Y.W. Li, W. Ren, S.L. Lin, G.X. Lu, J.H. Ye and Y.P. Bi, *Nanoscale*, 2013, **5**, 7552.

35 K. Naoi, Y. Ohko and T. Tatsuma, *J. Am. Chem. Soc.*, 2004, **126**, 3664.

36 X. F. Chu, T. Y. Chen, W. B. Zhang, B. Q. Zheng and H. F. Shui, *Sens. Actuators, B*, 2009, **142**, 49.

37 S.M. Wang, P. Wang, C.H. Xiao, B.B. Yao, R. Zhao and M.Z. Zhang, *CrystEngComm*, 2013, **15**, 9170.

38 W. Wen, J.M. Wu and Y.D. Wang, *Appl. Phys. Lett.*, 2012, **100**, 262111.

39 L.L. Wang, T. Fei, J.N. Deng, Z. Lou, R. Wang and T. Zhang, *J. Mater. Chem.*, 2012, **22**, 18111.

40 J.H. Lee, *Sens. Actuators, B*, 2009, **140**, 319.

41 X.J. Liu, Z. Chang, L. Luo, X.D. Lei, J.F. Liu and X.M. Sun, *J. Mater. Chem.*, 2012, **22**, 7232.

42 G.X. Zhu, Y.J. Liu, H. Xu, Y. Chen, X.P. Shen and Z. Xu, *CrystEngComm*, 2012, **14**, 719.